

Bit Rate Matching Algorithm Optimization in JPEG-AI Verification Model

Panqi Jia^{*†}, A. Burakhan Koyuncu^{†‡}, Jue Mao[‡], Ze Cui[‡], Yi Ma[‡], Tiansheng Guo[‡], Timofey Solovyev[‡], Alexander Karabutov[‡], Yin Zhao[‡], Jing Wang[‡], Elena Alshina[‡], André Kaup^{*}

^{*}Multimedia Communications and Signal Processing, Friedrich-Alexander University Erlangen-Nürnberg, Germany

[†]Chair of Media Technology, Technical University of Munich, Germany

[‡]Huawei Technologies

Abstract—The research on neural network (NN) based image compression has shown superior performance compared to classical compression frameworks. Unlike the hand-engineered transforms in the classical frameworks, NN-based models learn the non-linear transforms providing more compact bit representations, and achieve faster coding speed on parallel devices over their classical counterparts. Those properties evoked the attention of both scientific and industrial communities, resulting in the standardization activity JPEG-AI. The verification model for the standardization process of JPEG-AI is already in development and has surpassed the advanced VVC intra codec. To generate reconstructed images with the desired bits per pixel and assess the BD-rate performance of both the JPEG-AI verification model and VVC intra, bit rate matching is employed. However, the current state of the JPEG-AI verification model experiences significant slowdowns during bit rate matching, resulting in suboptimal performance due to an unsuitable model. The proposed methodology offers a gradual algorithmic optimization for matching bit rates, resulting in a fourfold acceleration and over 1% improvement in BD-rate at the base operation point. At the high operation point, the acceleration increases up to sixfold.

Index Terms—Learned Image Compression, JPEG-AI, bit rate matching, algorithm optimization

I. INTRODUCTION

The increasing demand on online media content drives development of efficient image compression techniques, where the goal is to produce compact image representations with as high-visual quality as possible. The compression algorithms can broadly be categorized into two groups: classical and neural network (NN)-based codecs. The classical codecs, such as JPEG [1], JPEG2000 [2], HEVC [3], BPG [4], and VVC intra [5], achieve this goal by following the pipeline of the transform coding [6]. They apply fixed transforms on image blocks, quantize the transformed vectors, and code them into a bitstream with a lossless entropy codec [7].

In recent years, various NN-based compression algorithms have been investigated to achieve better compression performance [8]–[18]. Those algorithms are based on non-linear transform coding [19] using an autoencoder-based architecture with non-linear transforms, which maps the input image to a compact latent representation. The transform coefficients are learned end-to-end along with an entropy model estimating the entropy of the latent variables. Early proposals [8]–

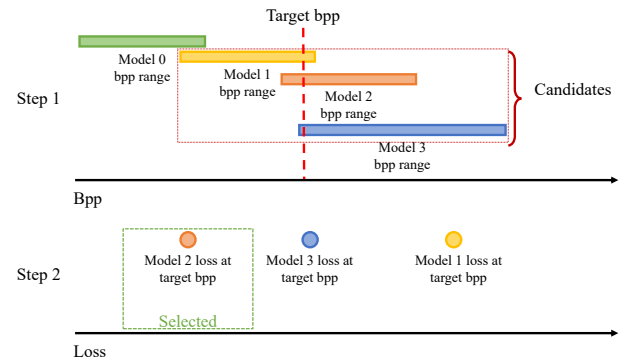


Fig. 1: Two steps of the model selection in the prior art

[12] reach a compression performance on par with classical codecs such as JPEG [1], JPEG2000 [2], and BPG [4]. More recent approaches [13]–[18] introduce transform layers with sophisticated activation functions [16], [18], and entropy model techniques with attention modules [13]–[15], [17], [18]. Those works surpass the compression performance of VVC intra [5], and even match the runtime complexity of the classical codecs [16]–[18]. However, they can only achieve multiple compression rates by training separate models for each rate point and cannot provide continuous variable rates with each single model during evaluation.

To achieve continuous variable rate coding, various modifications have been proposed to the NN-based compression algorithms [20]–[24]. For instance, Choi et al. [20] and Song et al. [21] introduce conditional transform layers, where the transforms are adaptively modified according to the target rate. Moreover, the model of [21] can allocate more bits for the region of interest to increase coding quality on a selected location. F. Brand et al. [22] proposed a pyramidal NN structure with latent masking. Finetuning the mask for each layer allows for variable rate coding. Alternatively, the model of [23], [24] proposes, a so called *gain unit*, which directly adjusts the latent variables without requiring modifications to the transform layers. The gain unit proposed is a trainable matrix that contains multiple gain vectors. Each gain vector provides a channel-wise quantization map, which

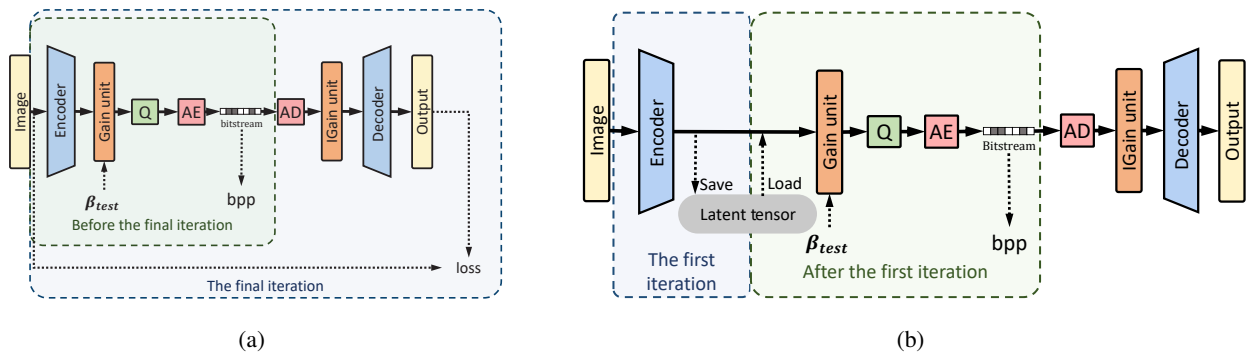


Fig. 2: β_{test} validation process (a) in prior art and (b) in our simplified method

offers different quantization steps for each channel. Different gain vectors can provide different discrete overall quantization steps to achieve a variable rate. Furthermore, by extrapolating or interpolating the gain vectors, the codec can achieve a continuous variable rate.

The recent standardization activity, JPEG-AI [25] has been investigating efficient NN-based codecs due to their notable compression performance. They released a verification model (VM) 4.1, where the model architecture is based on the conditional color separation (CCS) framework proposed in [26]. VM 4.1 has two operation points to support different complexity requirements. The high operation point (HOP) reaches a significantly high compression performance over VVC intra [5], whereas the base operation point (BOP) provides a moderate performance gain with a significantly lower model and runtime complexity. Moreover, VM 4.1 employs a gain unit similar to [23] in order to support continuous variable rate coding. This functionality also enables bit rate matching (BRM), where the scaling parameters for the gain unit vectors are iteratively optimized to match a given target bit per pixel (bpp). Since BRM requires an iterative algorithm, it has a significant runtime complexity. In this work, we propose novel optimization techniques for BRM, which provide up to 6.3 times lower runtime complexity and over 1% better compression gain over the existing BRM method.

II. BIT RATE MATCHING IN THE JPEG-AI VERIFICATION MODEL

To cover the large bpp range, JPEG-AI VM 4.1 employs five models trained for a specific Lagrange multiplier β_{train} determining rate-distortion trade-off [19]. A higher value of β_{train} yields a higher quality reconstructed image, requiring more bits to code. Each model uses a dedicated gain unit [23] to support continuous variable rate coding. To achieve the variable rate functionality for a single model, the model is provided with a test variable β_{test} during the testing. The selection methodology for β_{test} is explained in the following sections. Then, β_{test} is used to compute the displacement $\delta_\beta = \frac{\beta_{test}}{\beta_{train}}$, which is the scaling parameter of gain vectors in the gain unit. This scaling parameter can assist the gain unit in extrapolating to achieve a variable overall quantization level.

In the JPEG-AI requirement, the BRM condition is considered to be satisfied, if the generated bpp differs from the target bpp by less than 10%. In JPEG-AI VM4.1, the BRM consists of three parts: model selection, β_{test} searching, and β_{test} validation. In the model selection stage, BRM must locate the particular model that offers the target bpp. In the β_{test} searching phase, the ultimate β_{test} is determined for the selected model. In the β_{test} validation phase, the codec computes the bpp and loss for the β_{test} . This section provides a detailed account of each BRM step.

A. Model Selection

The BRM within JPEG-AI VM4.1 selects the candidate model with the minimum loss. This model indicates the bpp range that can cover the target bpp. Different minimum and maximum β_{test} are allocated for each model by the codec. Therefore, each model can offer a specific bpp range by utilizing the minimum and maximum β_{test} . If the target bpp is located within the bpp range of one model, then that model will be chosen as the candidate model. If the target bpp falls within the overlapping areas of multiple models' bpp ranges, then they will all be considered as candidates. Step 1 in Fig. 1 illustrates the chosen candidates.

Once the chosen candidate models have been identified, each model must seek out its respective β_{test} to achieve the target bpp. This is demonstrated in step 2 of Fig. 1, and the algorithm for the search for the β_{test} is presented in subsection II-B. Once the relevant β_{test} is found for each candidate model, the corresponding loss of that β_{test} is also determined. The loss is determined by comparing the reconstructed image with the original image and is a combination of the Mean Squared Error (MSE) [27] and the Multi-Scale Structural Similarity (MS-SSIM) [28] loss with varying weights. Ultimately, the model with the lowest loss and its corresponding β_{test} will be chosen.

B. β_{test} Searching for Single Model

In the model selection, each proposed model must identify the final β_{test} required to attain the target bpp. However, the model lacks knowledge of the ultimate destination of β_{test} . It only has access to the minimum and maximum

β_{test} values, which define the minimum and maximum bpp. Thus, the binary search is employed in this scenario. At each search iteration, the new β_{test} is updated as $\beta_{test} = \sqrt{\beta_{test_max} \times \beta_{test_min}}$. After each iteration, the new minimum and maximum β_{test} are updated by examining the bpp range that can cover the target bpp. The revised minimum β_{test} can generate the closest bpp to the target bpp in the bpp range that is below the target bpp. The updated maximum β_{test} can generate the closest bpp to the target bpp in the bpp range that is above the target bpp. The β_{test} is continually updated until it has reached the target bpp.

C. β_{test} Validation

Fig. 2a shows the validation process for β_{test} . During the β_{test} search, several β_{test} s require validation in candidate models. Two scenarios exist for β_{test} validation: when the β_{test} is unable to produce the desired bpp and when the β_{test} can supply bpp that approximates the target bpp. For both cases, the encoder must run in its entirety to obtain the latent tensor. Once the β_{test} has been applied to the latent tensor, the modified tensor goes to the entropy model to generate the bpp. If the bpp is not sufficiently close to the target bpp, the validation will cease, and the next β_{test} will be updated. Conversely, if the bpp is within range of the target bpp, the decoder will run to reconstruct the image for loss calculation. This loss calculation is used for selecting the model from the candidates.

III. PROPOSED ALGORITHM

In this section, we present our novel BRM optimization algorithm. Our algorithm optimises all three parts of the BRM and is introduced in the following subsections, where optimization of each part will be explained.

A. Relative Bit Distance Based Model Selection

In the field of model selection, various models are considered as candidates, and the ultimate model chosen is the one with the least loss. Nevertheless, this approach presents two drawbacks. Firstly, if there are numerous candidates, each candidate requires a β_{test} searching process for the target bpp, which is very time-consuming. Secondly, each candidate needs to calculate the loss in the end, prolonging the runtime of the decoder and metric calculation.

The combination of five models with $\delta_\beta = 1$ presents the optimal variable rate envelope. If δ_β deviates significantly from 1, the resulting rate-distortion curve diverges from the ideal envelope. Fig. 3 depicts the ideal envelope for all five models (represented by the orange curve), and the rate-distortion curve of a single model (depicted by the blue and green curve), which is trained for $\beta_{train} = 0.015$ and tested for different δ_β values. Notably, $\delta_\beta > 1$ causes a bigger discrepancy from the ideal envelope than using $\delta_\beta < 1$.

Based on these observations, the model that has the closest default bpp to the target bpp should be used to achieve the desired bpp. If the default bpp of the chosen model is higher than the target bpp, it can still provide a smaller gap from

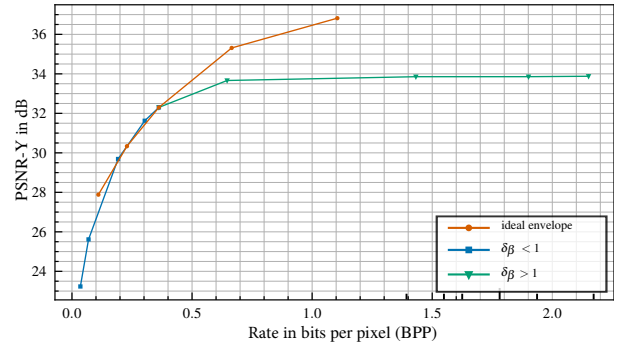


Fig. 3: Variable rate curve of a single model with different δ_β

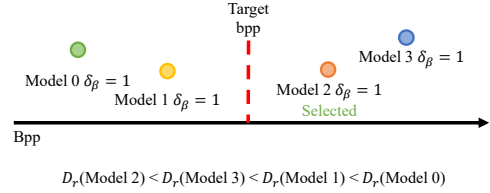


Fig. 4: Directly select model by comparing the D_r

the ideal envelope. We suggest using the relative bit distance $D_r = \text{abs}(bpp_{default} - bpp_{target}) / bpp_{default}$ as the evaluation criterion. The model with the minimum D_r to the target bpp will be selected directly. For instance, as illustrated in Fig. 4, the target bpp lies midway between the $bpp_{default}$ s of Model 1 and Model 2. The absolute difference in $bpp_{default}$ between the two models and the target bpp is identical. However, due to the higher $bpp_{default}$ of Model 2, its D_r is smaller. This model selection method generates a larger lower boundary than the upper boundary for the bpp range of each model. This non-symmetric boundary can result in variable rate performance that closely approximates the ideal envelope.

With the proposed model selection optimization, all models need to be calculated only once for the default bpp, and beta searching occurs only for the selected model. Additionally, the loss calculation is not necessary for this optimization. By simplifying the model selection strategy, significant runtime is saved.

B. β_{test} Searching Based on Linear Function

When searching for the appropriate β_{test} to achieve target bpp in prior art, the binary search method is utilized due to the ambiguous connection between β_{test} and bpp. Nevertheless, our statistical analysis revealed a proper approach to model the relationship between β_{test} and bpp.

In Fig. 5, the graph displays the natural logarithm of β_{test} and bpp . The logarithmic relationship between $\log(\beta_{test})$ and $\log(bpp)$ is approximately linear, allowing us to hypothesize that $\log(bpp) = A \cdot \log(\beta_{test}) + B$. In the initial iteration of β_{test} search, we calculate two parameters, A and B, by using the minimum and maximum β_{test} values along with their corresponding bpp. Then, we determine β_{test_1} by setting the

TABLE I: Average BD rate and run time of the original (org.) and the proposed (prop.) BRM methods applied on BOP and HOP models of JPEG-AI VM4.1.

Model	AVG	RunTime	BRMTime	BitDiff	MSSSIM	VIF	FSIM	NLPD	IWSSIM	VMAF	PSNRHVS
VTM 11.1	0.0%	–	–	10%	0.0%	0.0%	0.0%	0.0%	0.0%	0.0%	0.0%
BOP (tools off)	-11.0%	29 min	–	315%	-29.1%	-1.7%	-13.4%	-10.3%	-25.1%	-1.2%	3.4%
+ BRM (org.)	-8.1%	49 min	20 min	6%	-26.3%	-1.2%	-7.5%	-6.6%	-21.7%	0.7%	6.2%
+ BRM (prop.)	-9.2%	34 min	5 min	4%	-26.9%	-2.1%	-10.7%	-8.2%	-22.8%	0.6%	5.8%
HOP (tools off)	-25.7%	48 min	–	366%	-39.2%	-16.8%	-27.5%	-24.6%	-36.4%	-23.2%	-12.2%
+ BRM (org.)	-22.1%	282 min	234 min	9%	-35.6%	-15.0%	-21.9%	-21.1%	-32.6%	-19.9%	-8.5%
+ BRM (prop.)	-22.1%	85 min	37 min	4%	-35.4%	-15.3%	-21.9%	-21.1%	-32.4%	-19.7%	-8.6%

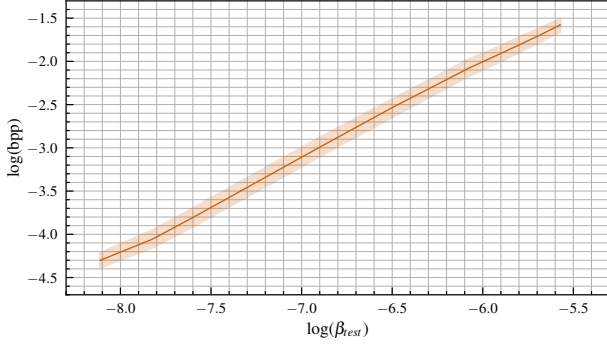


Fig. 5: Relationship between $\log(bpp)$ and $\log(\beta_{test})$

linear function of $\log(bpp) = \log(bpp_{target})$. We subsequently validate β_{test_1} in order to obtain bpp_{test_1} . If bpp_{test_1} is close enough to the bpp_{target} , the search process will end. Otherwise, the linear function incorporating β_{test_min} , β_{test_1} and their associated bpp will be created anew. We repeat the preceding process until reaching a value close enough to the target bpp.

Using a linear function to fit the connection between β_{test} and bpp can decrease the number of iterations required to search for β_{test} . This approach provides a clear direction for locating the β_{test} .

C. β_{test} Validation simplification

In the prior art, as illustrated in Fig. 2a, the encoder had to operate for each iteration while searching for β_{test} , and the decoder had to run upon discovering a valid β_{test} to produce the loss.

Noting that β_{test} only affects the gain vector, which represents the channel-wise quantization map of the latent tensor, it follows that the latent tensor is unchanged before the gain vector is applied in each iteration. To prevent the repeated generation of the unmodified latent tensor, we suggest storing the unmodified latent tensor during the first iteration and retrieving it during ensuing iterations. This approach saves computational time for the encoder. Furthermore, our proposed approach eliminates the need to compare all possible candidates during model selection, thereby preventing the need for loss calculation. By avoiding the calculation of the loss function, we can significantly reduce the runtime required for the decoder and metric calculations. The simplified β_{test} validation is illustrated in Fig. 2b.

IV. EXPERIMENTAL RESULTS

To assess the efficacy of our methodology, we compare it with JPEG-AI VM4.1. To accurately measure the BRM runtime, we initially carry out the tool-off configuration without BRM and record the runtime T_A . Next, for prior art, we enable BRM on top of the tool-off configuration and record the runtime T_B . The difference $T_B - T_A$ denotes the BRM runtime of the prior art. Our proposed method was implemented on a tool-off configuration and the resulting run time $T_C - T_A$ was recorded. To ensure consistent test conditions, we used a single NVIDIA Titan RTX graphics processing unit (GPU) with 24GB memory for all tests. Five target bpp points were evaluated: 0.06, 0.12, 0.25, 0.5, and 0.75 bpp. The models used for BRM were trained with beta values of 0.002, 0.007, 0.015, and 0.05. The δ_β ranges for each model were [0.1, 2.0], [0.3, 1.4], [0.4, 2], and [0.6, 6.0]. To test tool-off configuration without BRM, δ_β equal to 1 are used for each individual model. Furthermore, for the high rate range (0.75 bpp), we apply a δ_β equal to 2 for the last model. The results of the BRM are presented in Table I. The VVC Test Model (VTM 11.1) is used as the performance anchor in the table for VVC intra. Additionally, FFMPEG [29] will be used to convert the PNG (RGB) to YUV following the BT.709 primaries to generate the YUV format for metric calculation.

All experiments were conducted on the JPEG-AI Common and Training Test Conditions (CTTC) [30] test dataset, comprising 50 images with natural content. To evaluate the metrics, we computed the average Bjøntegaard Delta rate (BD-Rate) [31] performance across 7 metrics, including MSSSIM [28], Visual Information Fidelity (VIF) [32], feature similarity (FSIM) [33], Normalized Laplacian Pyramid (NLPD) [34], Information Content Weighted Structural Similarity Measure (IW-SSIM) [35], Video Multimethod Assessment Fusion (VMAF) [36], and PSNR-HVS-M [37]. Furthermore, we recorded the bit difference for determining the accuracy of BRM.

For the base operation point (BOP) of relatively lower complexity, our novel BRM exhibits a 5-minute runtime and an average BD-rate gain of -9.2% compared to VVC intra. In contrast, the BRM of the prior art has a runtime of 20 minutes and a gain of -8.1% over VVC. Therefore, our novel BRM achieves a 4 times increase in speed and a -1.1% improvement in BD-Rate when compared to the prior art in JPEG-AI VM4.1 over VVC intra. Similarly, for the high operation point (HOP)

with greater complexity, our novel BRM has a run time of 37 minutes and achieves a BD-rate gain of -22.1% over VVC intra. In comparison, the BRM in the prior art has a run time of 234 minutes and achieves a BD-rate gain of -22.1% over VVC intra. In summary, our novel BRM leads to a 6.3-fold enhancement in speed and attains similar average BD-rate proficiency to the prior art in JPEG-AI VM4.1 over VVC intra.

V. CONCLUSION

In this paper, we propose a novel BRM approach on top of JPEG-AI VM4.1, comprising relative bit distance-based model selection, linear function-based β_{test} searching, and non-decoder required β_{test} validation.

Compared to the BRM in JPEG-AI VM 4.1 over VVC intra, the proposed BRM for the base operation point achieves a -1.1% improvement in BD-rate and a 4-fold increase in speed. For the high operation point, the proposed BRM has an average BD-rate performance that is equivalent and provides a 6.3 times increase in speed.

REFERENCES

- [1] G. Wallace, "The JPEG still picture compression standard," *IEEE Transactions on Consumer Electronics*, vol. 38, no. 1, pp. xviii–xxxiv, 1992.
- [2] A. Skodras, C. Christopoulos, and T. Ebrahimi, "The JPEG 2000 still image compression standard," *IEEE Signal Processing Magazine*, vol. 18, no. 5, pp. 36–58, 2001.
- [3] G. J. Sullivan, J.-R. Ohm, W.-J. Han, and T. Wiegand, "Overview of the High Efficiency Video Coding (HEVC) Standard," *IEEE Transactions on Circuits and Systems for Video Technology*, vol. 22, no. 12, pp. 1649–1668, 2012.
- [4] F. Bellard, "BPG image format," 2015, accessed: 2021-11-05. URL <https://bellard.org/bpg>.
- [5] B. Bross, Y.-K. Wang, Y. Ye, S. Liu, J. Chen, G. J. Sullivan, and J.-R. Ohm, "Overview of the Versatile Video Coding (VVC) Standard and its Applications," *IEEE Transactions on Circuits and Systems for Video Technology*, vol. 31, no. 10, pp. 3736–3764, 2021.
- [6] V. K. Goyal, "Theoretical foundations of transform coding," *IEEE Signal Processing Magazine*, vol. 18, no. 5, pp. 9–21, 2001.
- [7] J. Rissanen and G. G. Langdon, "Arithmetic coding," *IBM Journal of Research and Development*, vol. 23, no. 2, pp. 149–162, 1979.
- [8] J. Ballé, V. Laparra, and E. P. Simoncelli, "End-to-end Optimized Image Compression," *ArXiv*, vol. abs/1611.01704, 2017.
- [9] J. Ballé, D. Minnen, S. Singh, S. J. Hwang, and N. Johnston, "Variational image compression with a scale hyperprior," *ArXiv*, vol. abs/1802.01436, 2018.
- [10] D. Minnen, J. Ballé, and G. Toderici, "Joint Autoregressive and Hierarchical Priors for Learned Image Compression," *ArXiv*, vol. abs/1809.02736, 2018.
- [11] Z. Cheng, H. Sun, M. Takeuchi, and J. Katto, "Learned image compression with discretized gaussian mixture likelihoods and attention modules," in *Proc. IEEE/CVF Conference on Computer Vision and Pattern Recognition (CVPR)*, 2020, pp. 7939–7948.
- [12] A. B. Koyuncu, K. Cui, A. Boev, and E. Steinbach, "Parallelized context modeling for faster image coding," in *2021 International Conference on Visual Communications and Image Processing (VCIP)*. IEEE, 2021, pp. 1–5.
- [13] Z. Guo, Z. Zhang, R. Feng, and Z. Chen, "Causal contextual prediction for learned image compression," *IEEE Transactions on Circuits and Systems for Video Technology*, 2021.
- [14] Y. Qian, X. Sun, M. Lin, Z. Tan, and R. Jin, "Entroformer: A transformer-based entropy model for learned image compression," in *International Conference on Learning Representations*, 2021.
- [15] A. B. Koyuncu, H. Gao, A. Boev, G. Gaikov, E. Alshina, and E. Steinbach, "Contextformer: A transformer with spatio-channel attention for context modeling in learned image compression," in *European Conference on Computer Vision*. Springer, 2022, pp. 447–463.
- [16] D. He, Z. Yang, W. Peng, R. Ma, H. Qin, and Y. Wang, "Elic: Efficient learned image compression with unevenly grouped space-channel contextual adaptive coding," in *Proceedings of the IEEE/CVF Conference on Computer Vision and Pattern Recognition*, 2022, pp. 5718–5727.
- [17] A. B. Koyuncu, P. Jia, A. Boev, E. Alshina, and E. Steinbach, "Efficient contextformer: Spatio-channel window attention for fast context modeling in learned image compression," 2023.
- [18] J. Liu, H. Sun, and J. Katto, "Learned image compression with mixed transformer-cnn architectures," in *Proceedings of the IEEE/CVF Conference on Computer Vision and Pattern Recognition*, 2023, pp. 14 388–14 397.
- [19] J. Ballé, P. A. Chou, D. Minnen, S. Singh, N. Johnston, E. Agustsson, S. J. Hwang, and G. Toderici, "Nonlinear transform coding," *IEEE Journal of Selected Topics in Signal Processing*, vol. 15, no. 2, pp. 339–353, 2020.
- [20] Y. Choi, M. El-Khamy, and J. Lee, "Variable rate deep image compression with a conditional autoencoder," 2019.
- [21] M. Song, J. Choi, and B. Han, "Variable-rate deep image compression through spatially-adaptive feature transform," in *Proceedings of the IEEE/CVF International Conference on Computer Vision*, 2021, pp. 2380–2389.
- [22] F. Brand, K. Fischer, and A. Kaup, "Rate-distortion optimized learning-based image compression using an adaptive hierarchical autoencoder with conditional hyperprior," in *2021 IEEE/CVF Conference on Computer Vision and Pattern Recognition Workshops (CVPRW)*, 2021, pp. 1885–1889.
- [23] Z. Cui, J. Wang, B. Bai, T. Guo, and Y. Feng, "G-vae: A continuously variable rate deep image compression framework," *ArXiv*, vol. abs/2003.02012, 2020. [Online]. Available: <https://api.semanticscholar.org/CorpusID:211988449>
- [24] Z. Cui, J. Wang, S. Gao, T. Guo, Y. Feng, and B. Bai, "Asymmetric gained deep image compression with continuous rate adaptation," in *Proceedings of the IEEE/CVF Conference on Computer Vision and Pattern Recognition*, 2021, pp. 10 532–10 541.
- [25] J. Ascenso, E. Alshina, and T. Ebrahimi, "The jpeg ai standard: Providing efficient human and machine visual data consumption," *IEEE MultiMedia*, vol. 30, no. 1, pp. 100–111, 2023.
- [26] P. Jia, A. B. Koyuncu, G. Gaikov, A. Karabutov, E. Alshina, and A. Kaup, "Learning-based conditional image coder using color separation," in *2022 Picture Coding Symposium (PCS)*, 2022, pp. 49–53.
- [27] J. Søgaard, L. Krasula, M. Shahid, D. Temel, K. Brunnström, and M. Razaak, "Applicability of existing objective metrics of perceptual quality for adaptive video streaming," in *Image Quality and System Performance*, 2016. [Online]. Available: <https://api.semanticscholar.org/CorpusID:26253431>
- [28] Z. Wang, E. Simoncelli, and A. Bovik, "Multiscale structural similarity for image quality assessment," in *The Thirty-Seventh Asilomar Conference on Signals, Systems & Computers*, 2003, vol. 2, 2003, pp. 1398–1402 Vol.2.
- [29] S. Tomar, "Converting video formats with ffmpeg," *Linux Journal*, vol. 2006, no. 146, p. 10, 2006.
- [30] C. Subgroup, "JPEG AI – Learning-based Image coding Common and Training Test Conditions," 2023, ISO/IEC JTC 1/SC29/WG1 N100600, JPEG AI (ISO/IEC 6048).
- [31] G. Bjontegaard, "Calculation of average PSNR differences between RD-curves," *VCEG-M33*, 2001.
- [32] H. Sheikh and A. Bovik, "Image information and visual quality," vol. 3, 01 2004, pp. iii–709.
- [33] L. Zhang, L. Zhang, X. Mou, and D. Zhang, "Fsim: A feature similarity index for image quality assessment," *IEEE Transactions on Image Processing*, vol. 20, no. 8, pp. 2378–2386, 2011.
- [34] V. Laparra, J. Ballé, A. Bernardino, and E. Simoncelli, "Perceptual image quality assessment using a normalized laplacian pyramid," *Electronic Imaging*, vol. 2016, pp. 1–6, 02 2016.
- [35] Z. Wang and Q. Li, "Information content weighting for perceptual image quality assessment," *IEEE Transactions on Image Processing*, vol. 20, no. 5, pp. 1185–1198, 2011.
- [36] Z. Li, A. Aaronand, I. Katsavounidis, A. Moorthy, and M. Manohara, "Toward A Practical Perceptual Video Quality Metric," 2016, <https://netflixtechblog.com/toward-a-practical-perceptual-video-quality-metric-653f208b9652>.
- [37] N. Ponomarenko, F. Silvestri, K. Egiazarian, M. Carli, J. Astola, and V. Lukin, "On between-coefficient contrast masking of dct basis func-

tions," *Proc of the 3rd Int Workshop on Video Processing and Quality Metrics for Consumer Electronics*, 01 2007.